

# UC San Diego

## UC San Diego Previously Published Works

### Title

3D adiabatic T1ρ prepared ultrashort echo time cones sequence for whole knee imaging

### Permalink

<https://escholarship.org/uc/item/0t48s5gm>

### Journal

Magnetic Resonance in Medicine, 80(4)

### ISSN

0740-3194

### Authors

Ma, Ya-Jun  
Carl, Michael  
Searleman, Adam  
[et al.](#)

### Publication Date

2018-10-01

### DOI

10.1002/mrm.27131

Peer reviewed

# 3D adiabatic $T_{1\rho}$ prepared ultrashort echo time cones sequence for whole knee imaging

Ya-Jun Ma<sup>1</sup> | Michael Carl<sup>2</sup> | Adam Searleman<sup>1</sup> | Xing Lu<sup>1</sup> | Eric Y. Chang<sup>1,3</sup> | Jiang Du<sup>1</sup>

<sup>1</sup>Department of Radiology, University of California, San Diego, California

<sup>2</sup>GE Healthcare, San Diego, California

<sup>3</sup>Radiology Service, VA San Diego Healthcare System, San Diego, California

## Correspondence

Jiang Du, University of California, San Diego, Department of Radiology, 200 West Arbor Drive, San Diego, CA 92103-8226.  
Email: jiangdu@ucsd.edu

## Funding information

GE Healthcare; National Institutes of Health, Grant/Award Numbers: T32EB005970, 1R01 AR062581, and 1R01 AR068987; VA Clinical Science R&D Service, Grant/Award Number: 1101CX001388

**Purpose:** To develop a 3D adiabatic  $T_{1\rho}$  prepared ultrashort echo time cones (3D Adiab $T_{1\rho}$  UTE-Cones) sequence for whole knee imaging on a clinical 3T scanner.

**Methods:** A train of adiabatic full passage pulses were used for spin locking, followed by time-efficient multispoke UTE acquisition to detect signals from both short and long  $T_2$  tissues in the whole knee joint. A modified signal model was proposed for multispoke UTE data fitting. The feasibility of this 3D Adiab $T_{1\rho}$  UTE-Cones technique was demonstrated through numerical simulation, phantom, and ex vivo knee sample studies. The 3D Adiab $T_{1\rho}$  UTE-Cones technique was then applied to 6 in vivo knee joints of healthy volunteers to measure  $T_{1\rho}$  values of quadriceps tendon, patellar tendon, anterior cruciate ligament (ACL), posterior cruciate ligament (PCL), meniscus, patellar cartilage, and muscle.

**Results:** Numerical simulation, phantom and ex vivo knee sample studies demonstrated the feasibility of whole knee imaging using the proposed multispoke 3D Adiab $T_{1\rho}$  UTE-Cones sequence. The healthy volunteer knee study demonstrated an averaged  $T_{1\rho}$  of  $13.9 \pm 0.7$  ms for the quadriceps tendon,  $9.7 \pm 0.8$  ms for the patellar tendon,  $34.9 \pm 2.8$  ms for the ACL,  $21.6 \pm 1.4$  ms for the PCL,  $22.5 \pm 1.9$  ms for the meniscus,  $44.5 \pm 2.4$  ms for the patellar cartilage, and  $43.2 \pm 1.1$  ms for the muscle.

**Conclusion:** The 3D Adiab $T_{1\rho}$  UTE-Cones sequence allows volumetric  $T_{1\rho}$  assessment of both short and long  $T_2$  tissues in the knee joint on a clinical 3T scanner.

## KEY WORDS

Adiab $T_{1\rho}$ , multispoke, ultrashort echo time, whole knee imaging

## 1 | INTRODUCTION

Quantitative MRI of spin lattice relaxation in the rotating frame ( $T_{1\rho}$ ) has been proposed as a biomarker of cartilage degeneration.<sup>1-4</sup> There is clinical interest in developing non-invasive biomarkers that are sensitive to the early degenerative changes in cartilage, including loss of proteoglycans (PGs) and changes in collagen, for the early diagnosis of osteoarthritis (OA).<sup>1</sup> It has been shown that  $T_{1\rho}$  increases

with cartilage degeneration,<sup>5-7</sup> and spin lock at different frequencies has been used to detect changes in proteoglycans (PGs) or collagen.<sup>8,9</sup>

A strong magic angle effect is an important limitation of quantitative continuous-wave (CW)  $T_{1\rho}$  imaging of collagen-rich tissues such as cartilage, menisci, and ligaments.<sup>10-13</sup> The highly ordered collagen fibers in these tissues are subject to strong dipole-dipole interactions that are modulated by the term  $3\cos^2(\theta) - 1$ , where  $\theta$  is the angle between the fiber

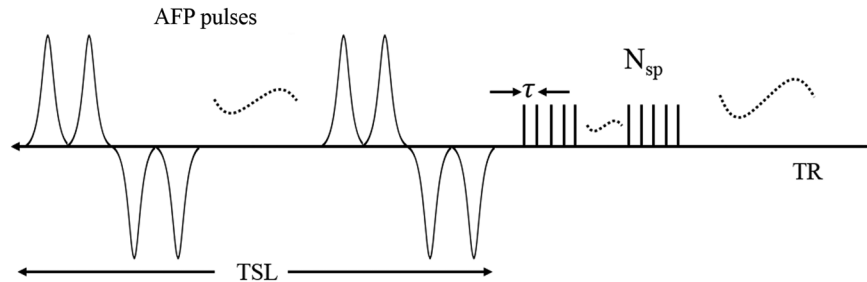


**FIGURE 1** The 3D Adiab $T_{1\rho}$  UTE-Cones sequence used a train of AFP pulses to generate  $T_{1\rho}$  contrast, followed by 3D UTE-Cones data acquisition. To speed up data acquisition, multiple spokes were sampled after each AFP pulse train

orientation and the main magnetic field  $\vec{B}_0$ .<sup>14</sup> Previous studies show that  $T_{1\rho}$  values can increase more than 200% in the middle and deep zones of articular cartilage and 300% in ligaments, when  $\theta$  is oriented from  $0^\circ$  to  $55^\circ$ .<sup>12,13</sup> The significant  $T_{1\rho}$  changes because of the magic angle effect make the evaluation of tissue degeneration extremely complicated.

Recently, a novel imaging technique was developed in which trains of adiabatic full passage (AFP) pulses are used to generate  $T_{1\rho}$  relaxation (Adiab $T_{1\rho}$ ).<sup>15–21</sup> Adiab $T_{1\rho}$  has been reported to be less sensitive to the magic angle effect compared with both CW- $T_{1\rho}$  and  $T_2$  relaxations in bovine cartilage studies.<sup>19,20</sup> Therefore, Adiab $T_{1\rho}$  may be a more reliable biomarker of PG loss in collagen-rich tissues than conventional CW- $T_{1\rho}$ . In addition, Adiab $T_{1\rho}$  has other advantages over CW spin-lock sequences. Most notably, adiabatic pulses are less sensitive to the spatial inhomogeneity of the transmit RF magnetic field compared with CW spin-lock pulses, and the flexibility of AFP pulse design allows moderation of RF power deposition.<sup>15,18,20,22</sup> Moreover, an extended range of frequencies or correlation times are effectively involved in the spin lattice relaxation when using AFP pulses, which may provide more information on the physicochemical mechanisms underlying pathological changes in tissues.

Human knee joints are composed of many different tissues including articular cartilage, calcified cartilage, menisci, ligaments, tendons, and bone, all of which are important for the health of the joint.<sup>23–25</sup> However, both CW- $T_{1\rho}$  and Adiab $T_{1\rho}$  measurements based on conventional MRI pulse sequences (such as GRE and FSE) are of limited value for detecting early PG depletion in short  $T_2$  tissues or tissue components such as the deep radial and calcified cartilage, menisci, ligaments, and tendons. These tissues or tissue components typically have  $T_2$ s ranging from sub-milliseconds to several milliseconds and therefore provide little or no detectable signal using conventional sequences.<sup>26–29</sup>

To overcome this challenge, we propose a combination of a 3D ultrashort echo time sequence using cones trajectories with an Adiab $T_{1\rho}$  preparation (3D Adiab $T_{1\rho}$  UTE-Cones) for volumetric  $T_{1\rho}$  assessment of both short and long  $T_2$  tissues in the knee joint on a clinical 3T scanner. The

details of 3D UTE-Cones sequence was described in the recent publications.<sup>30,31</sup> Multispoke acquisition after each Adiab $T_{1\rho}$  preparation was incorporated for time-efficiency. A modified signal model for multispoke acquisition was proposed for accurate  $T_{1\rho}$  fitting. Both simulation and phantom studies were carried out to investigate the accuracy of the modified signal model. Next, the magic angle effect was investigated by the repeated imaging of a sliced human patellar cartilage sample at 5 angular orientations from  $0^\circ$  to  $90^\circ$  relative to the  $\vec{B}_0$  field. Finally, the new sequence was applied to 4 ex vivo human knee joint specimens and 6 in vivo knee joints of healthy volunteers for  $T_{1\rho}$  measurements of quadriceps tendon, patellar tendon, anterior cruciate ligament (ACL), posterior cruciate ligament (PCL), meniscus, patellar cartilage, and muscle.

## 2 | THEORY

Features of the 3D Adiab $T_{1\rho}$  UTE-Cones pulse sequence used in this study are shown in Figure 1. An even number ( $N_{\text{AFP}}$ ) of AFP pulses are used for Adiab $T_{1\rho}$  preparation. When  $N_{\text{AFP}}$  is a multiple of 4, then every 4 consecutive AFP pulses follow a MLEV4 phase cycling scheme.<sup>32</sup> When  $N_{\text{AFP}}$  is equal to  $4n + 2$  ( $n = 0, 1, 2 \dots$ ), the first  $4n$  AFP pulses follow a MLEV4 phase cycling scheme, and the amplitude of the remaining 2 AFP pulses can be arbitrarily positive or negative because the AFP pulse can invert the spins robustly when the adiabatic condition is satisfied.<sup>15</sup> Here, we use 2 positive AFP pulses. Following the Adiab $T_{1\rho}$  preparation are  $N_{\text{sp}}$  separate k-space spokes or acquisitions with an equal time interval  $\tau$  for fast data acquisition.

The spin lock time TSL is defined as the total duration of the train of AFP pulses, i.e.,  $\text{TSL} = N_{\text{AFP}} \times T_p$  ( $T_p$  is the duration of a single AFP pulse). TR defined in this study is the duration between the adjacent Adiab $T_{1\rho}$  preparations. A relatively short TR (e.g., several hundred milliseconds) is used in the proposed sequence to accelerate data acquisition. At steady state, the signal equation is expressed as follows when a single acquisition ( $N_{\text{sp}} = 1$ ) is obtained after Adiab $T_{1\rho}$  preparation:<sup>27</sup>

$$S(\text{TSL}) = M_0 \sin(\alpha) \frac{e^{-\frac{\text{TSL}}{T_{1p}}} \left(1 - e^{-\frac{\text{TR} - \text{TSL}}{T_1}}\right)}{1 - e^{-\frac{\text{TSL}}{T_{1p}}} e^{-\frac{\text{TR} - \text{TSL}}{T_1}} \cos(\alpha)} + C. \quad (1)$$

Where  $M_0$  is the equilibrium state magnetization and  $\alpha$  is the excitation flip angle. A constant  $C$  is induced to account for non- $T_{1p}$  related factors such as background noise and artifacts associated with data acquisition and image reconstruction.

In our previous conventional CW- $T_{1p}$  study with 5 spokes per  $T_{1p}$  preparation, acceptable  $T_{1p}$  values were obtained by fitting the single spoke acquisition equation (Eq. 1).<sup>29</sup> However, Eq. 1 will introduce increasing error as the number of excitation spokes per Adiab $T_{1p}$  preparation increases (i.e.,  $N_{sp} > 5$ ) because it does not model the saturation effect induced by the multiple excitations. Therefore, similar to our recent multispoke MT modeling study, we modified the single spoke equation Eq. 1 by simply changing  $\cos(\alpha)$  to  $\cos^{N_{sp}}(\alpha)$  to account for the saturation effect of  $N_{sp}$  acquisitions, which is expressed as follows:<sup>33</sup>

$$S(\text{TSL}) = M_0 \sin(\alpha) \frac{e^{-\frac{\text{TSL}}{T_{1p}}} \left(1 - e^{-\frac{\text{TR} - \text{TSL}}{T_1}}\right)}{1 - e^{-\frac{\text{TSL}}{T_{1p}}} e^{-\frac{\text{TR} - \text{TSL}}{T_1}} \cos^{N_{sp}}(\alpha)} + C. \quad (2)$$

The motivation for Eq. 2 can be understood when considering a tissue with very long  $T_1$  relative to the spoke time interval  $\tau$ . In this case, the longitudinal magnetization will not substantially recover between consecutive excitations, resulting in progressive saturation between spokes. Therefore, the net behavior of the multispoke excitations is analogous to a single excitation with a flip angle of  $\arccos(\cos^{N_{sp}}(\alpha))$ . In contrast, Eq. 1 assumes a short enough  $T_1$  for the longitudinal magnetization to fully recover between each spoke. In practice, the  $T_1$  values of most tissues are much longer than the spoke time interval  $\tau$  (around 5 ms), so the signal model of Eq. 2 would be preferred. The 2 models were compared by simulation and phantom studies.

For both Eqs. 1 and 2, accurate  $T_1$  measurement is crucial for  $T_{1p}$  calculation. Here, a 3D UTE-Cones variable flip angle (VFA) method was used to measure  $T_1$  by fitting the following equation:<sup>34</sup>

$$S = M_0 \sin(\varphi) \frac{1 - e^{-\frac{\text{TR}}{T_1}}}{1 - e^{-\frac{\text{TR}}{T_1}} \cos(\varphi)}. \quad (3)$$

Where  $\varphi$  is the flip angle and TR is the repetition time. However, the VFA technique is very sensitive to  $B_1$  inhomogeneity. Therefore, a 3D dual-TR UTE-Cones sequence was also developed for actual flip angle imaging (UTE-Cones AFI)<sup>35</sup> to obtain a  $B_1$  scaling factor by dividing the measured actual flip angle by the nominal flip angle. With a known  $B_1$  scaling factor, the flip angle  $\varphi$  in Eq. 3 can be corrected for accurate  $T_1$  fitting. The  $B_1$  scaling factor value can also be used to correct  $\alpha$  in both Eqs. 1 and 2 for accurate

$T_{1p}$  measurement. No  $B_1$  correction is needed for Adiab $T_{1p}$  preparation because the AFP pulses are insensitive to  $B_1$  inhomogeneity.

### 3 | METHODS

The 3D Adiab $T_{1p}$  UTE-Cones sequence (see Figure 1) was implemented on a 3T whole body scanner (GE Healthcare Technologies, Milwaukee, WI). An 8-channel transmit/receive knee coil was used for both RF transmission and signal reception in the following experiments except as noted. The 3D UTE-Cones sequence used unique k-space trajectories that sampled data along evenly spaced twisting paths in the shape of multiple cones.<sup>31,32</sup> Data acquisition started as soon as possible after the RF excitation with a minimal nominal echo time of 32  $\mu\text{s}$ . The nominal echo time is defined as the time between the end of the rectangular pulse and the k-space center. Both RF and gradient spoiling were used to crush the remaining transverse magnetizations after each data acquisition. The RF spoiling method used here is to increase the RF phase quadratically with a phase increment factor of 117°. The  $T_2$ -weighted transverse magnetizations were crushed and will not contribute to steady-state signals. Identical non-selective AFP pulses (hyperbolic secant type 1 pulse) with a duration of 6.048 ms, bandwidth of 1.643 kHz and maximum  $B_1$  amplitude of 17  $\mu\text{T}$  were used to generate  $T_{1p}$  contrast.<sup>36</sup> Here, we used the shortest AFP pulse that can satisfy the adiabatic condition to increase the pulse bandwidth and get adequate TSLs for short  $T_2$  tissue imaging. A gradient following the train of Adiab $T_{1p}$  pulses was used to crush the remaining transverse magnetizations. The 3D Adiab $T_{1p}$  UTE-Cones sequence allows for anisotropic resolution (e.g., high in-plane resolution and thicker slices) for much improved SNR and reduced scan time relative to isotropic imaging.<sup>32,36</sup>

#### 3.1 | Simulation

Numerical simulation was carried out to investigate the accuracy of the fitting models of Eqs. 1 and 2 for multispoke acquisition. The simulated signal intensity of Adiab $T_{1p}$  preparation followed the mono-exponential function of  $e^{-\text{TSL}/T_{1p}}$ .<sup>18</sup> The  $T_1$  value was set to 1000 ms and the Adiab $T_{1p}$  UTE-Cones sequence parameters were shown as follows: TR = 500 ms, excitation flip angle = 10°, acquisition interval between adjacent spokes  $\tau = 5$  ms, the gap between the end of the last AFP pulse and start of the excitation pulse was 8 ms, each AFP pulse duration  $T_p = 6$  ms, and 8 different groups of AFP pulses in Adiab $T_{1p}$  preparation with  $N_{\text{AFP}} = 0, 2, 4, 6, 8, 12,$  and 16. Eleven groups of data were generated by Bloch equation simulation with different numbers of acquisition spokes:  $N_{sp} = 1, 5, 10, 15, 20,$

25, 30, 35, 40, 45, and 50. Both Eqs. 1 and 2 were used for data fitting.

### 3.2 | Phantom study

The phantom was prepared as 2% w/v agarose gel containing 0.1 mM MnCl<sub>2</sub>. In addition to the proposed 3D AdiabT<sub>1ρ</sub> UTE-Cones sequence, a 3D UTE-Cones AFI sequence and VFA UTE-Cones sequence were used for B<sub>1</sub> mapping and T<sub>1</sub> measurement, respectively. B<sub>1</sub> maps were used to correct both T<sub>1</sub> and T<sub>1ρ</sub> calculation. The phantom was scanned using the same field of view (FOV) of 12 × 12 × 8 cm<sup>3</sup> and receiver bandwidth of 166 kHz for all sequences. Other sequence parameters were: (1) 3D UTE-Cones AFI: TR<sub>1</sub>/TR<sub>2</sub> = 20/100 ms, flip angle = 45°, acquisition matrix of 64 × 64 × 20 and a total scan time of 5 min 30 s; (2) 3D VFA UTE-Cones: TR = 20 ms, flip angle = 5°, 10°, 20°, and 30°, acquisition matrix of 128 × 128 × 20 and a total scan time of 5 min 48 s; and (3) 3D AdiabT<sub>1ρ</sub> UTE-Cones: TR = 500 ms, flip angle = 10°, acquisition matrix of 128 × 128 × 20, and N<sub>AFP</sub> = 0, 2, 4, 6, 8, 12, and 16. Six groups of AdiabT<sub>1ρ</sub> data were acquired with different N<sub>sp</sub> of 1, 5, 15, 25, 35, and 45 per AdiabT<sub>1ρ</sub> preparation. The corresponding scan times were 253 min 59 s, 50 min 52 s, 17 min 23 s, 10 min 37 s, 7 min 49 s, and 6 min 11 s, respectively. Reproducibility of the proposed AdiabT<sub>1ρ</sub> method was investigated using the agarose phantom. The protocol was repeated 4 times with the MR system reset before each 3D AdiabT<sub>1ρ</sub> UTE-Cones scan.

### 3.3 | Magic angle effect study

Magic angle effect study for both T<sub>1ρ</sub> and T<sub>2</sub> was carried out by imaging a sliced human patellar sample (~4 mm thick) using a wrist coil (BC-10, Medspira, Minneapolis, MN) for both RF transmission and signal reception. The sample was imaged with 5 angular orientations (i.e., 0°, 30°, 55°, 70°, and 90°) with respect to the normal direction of cartilage surface. For each angular orientation, 3D AdiabT<sub>1ρ</sub> UTE-Cones and 2D Carr-Purcell-Meiboom-Gill (CPMG) sequences were used for T<sub>1ρ</sub> and T<sub>2</sub> measurements, respectively. The CPMG sequence is a multiple spin echo sequence to acquire a series of data with different echo times to quantitate T<sub>2</sub> value. The phase encoding and phase rewinder gradients in this sequence are balanced to refocus the stimulated echoes from imperfect 180° pulses at the same time as the spin echoes. Because tissue T<sub>1</sub> is not sensitive to the magic angle effect, T<sub>1</sub> measurement with a 2D inversion recovery prepared fast spin echo (IR-FSE) sequence was performed only at angle 0°. A chemical shift saturation (FatSat) module (8 ms) located between AdiabT<sub>1ρ</sub> preparation and the data acquisition was used for fat suppression. The sequence parameters were: (1) 3D AdiabT<sub>1ρ</sub> UTE-Cones with FatSat:

FOV = 5 × 5 × 2 cm<sup>3</sup>, acquisition matrix of 128 × 128 × 10, receiver bandwidth = 83.3 kHz, TR = 1000 ms, flip angle = 10°, N<sub>sp</sub> = 5, and N<sub>AFP</sub> = 0, 4, 8, 12, 16 and 20 each with a scan time of 6 min 45 s; (2) 2D CPMG with FatSat: FOV = 5 × 5 cm<sup>2</sup>, acquisition matrix of 192 × 128, slice thickness = 4 mm, TR = 3000 ms, flip angle = 90°, TEs = 10.7, 21.3, 32.0, 43.7, 53.4, 64.0, 74.7, and 85.4 ms; and (3) 2D IR-FSE: FOV = 5 × 5 cm<sup>2</sup>, acquisition matrix of 192 × 128, slice thickness = 4 mm, TR = 5000 ms, flip angle = 90°, TEs = 10.7 ms, and TIs = 50, 150, 300, 500, 700, 1000, 1500, 2000, and 3000 ms.

### 3.4 | Ex vivo knee study

High resolution whole knee imaging was performed on 4 knee samples from 4 donors (51–79 years of age, mean age 61.5 years; 1 male, 3 females). 3D UTE-Cones AFI, VFA, and AdiabT<sub>1ρ</sub> UTE-Cones sequences were used to scan these knee samples using a common FOV of 15 × 15 × 12 cm<sup>3</sup> and receiver bandwidth of 166 kHz. Other sequence parameters were: (1) 3D UTE-Cones AFI: TR<sub>1</sub>/TR<sub>2</sub> = 20/100 ms, flip angle = 45°, acquisition matrix of 128 × 128 × 30, and a total scan time of 10 min 54 s; (2) 3D VFA UTE-Cones: TR = 24 ms, flip angle = 4°, 8°, 16°, 24°, 32°, and 40°, acquisition matrix of 256 × 256 × 60, and a total scan time of 8 min 19 s; and (3) 3D AdiabT<sub>1ρ</sub> UTE-Cones with FatSat: TR = 500 ms, flip angle = 10°, acquisition matrix of 256 × 256 × 60, N<sub>sp</sub> = 21, and N<sub>AFP</sub> = 0, 2, 4, 6, 8, 12, 16, and 20 each with a scan time of 8 min 19 s.

### 3.5 | In vivo knee study

In vivo whole knee imaging was carried out on 6 healthy volunteers (23–42 years of age, mean age 30.3 years; 4 males, 2 females). Informed consent was obtained from all subjects in accordance with guidelines of the institutional review board. 3D UTE-Cones AFI, VFA, and AdiabT<sub>1ρ</sub> UTE-Cones sequences were used to scan these knees, using a common FOV of 15 × 15 × 10.8 cm<sup>3</sup> and receiver bandwidth of 166 kHz. Other sequence parameters were: (1) 3D UTE-Cones AFI: TR<sub>1</sub>/TR<sub>2</sub> = 20/100 ms, flip angle = 45°, acquisition matrix of 128 × 128 × 18, acquisition stretch factor of 1.4, and a total scan time of 4 min 57 s; (2) 3D VFA UTE-Cones: TR = 20 ms, flip angle = 5°, 10°, 20°, and 30°, acquisition matrix of 256 × 256 × 36, undersampling factor of 0.9, acquisition stretch factor of 1.4 and a total scan time of 9 min 28 s; and (3) 3D AdiabT<sub>1ρ</sub> UTE-Cones with FatSat: TR = 500 ms, flip angle = 10°, acquisition matrix of 256 × 256 × 36, acquisition stretch factor of 1.6, N<sub>sp</sub> = 25, and N<sub>AFP</sub> = 0, 2, 4, 6, 8, 12, and 16 each with a scan time of 2 min 34 s.

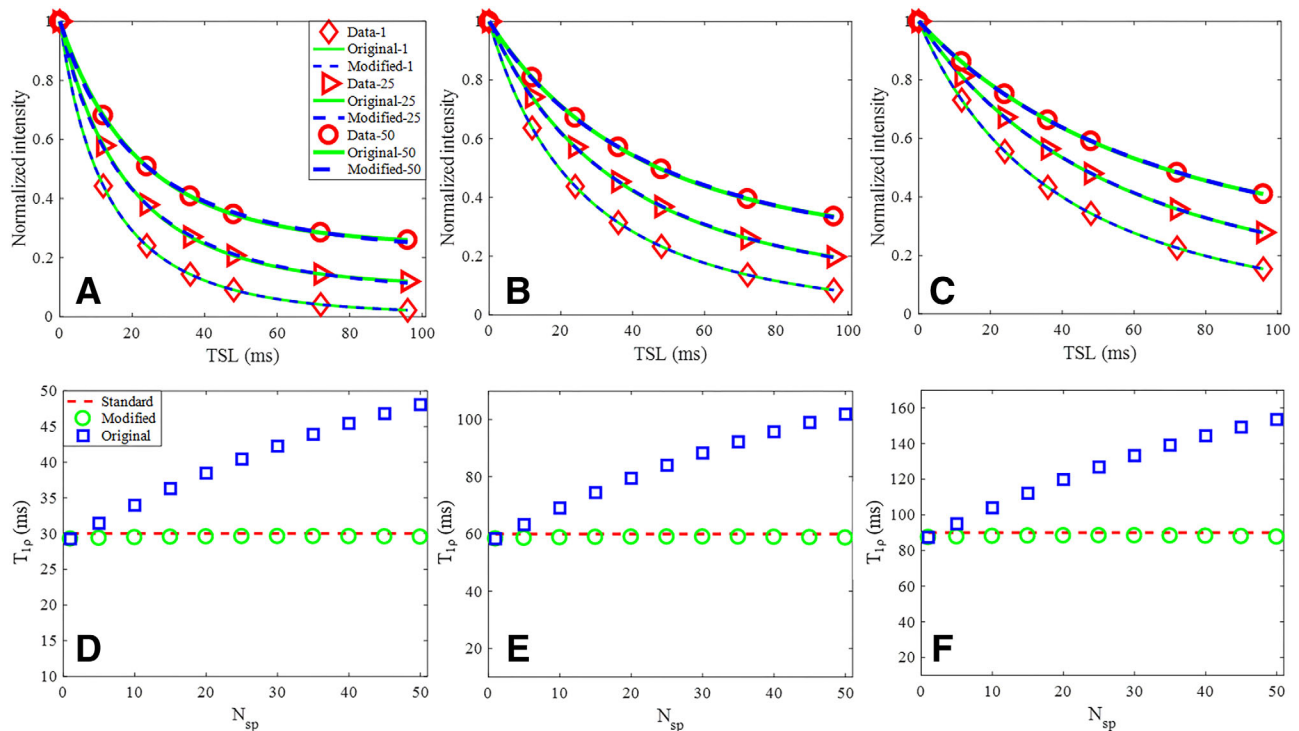


**FIGURE 2** Comparison of multispoke fitting models by simulation. (A–C) Bloch equation simulated data with corresponding fitting curves of both original (Eq. 1) and modified (Eq. 2) signal models. Each series data with a specific  $N_{sp}$  was normalized. The red diamond, triangle, and circle markers represented the simulated data with 1, 25, and 50 spokes per Adiab $T_{1\rho}$  preparation, respectively. (D–F) Calculated  $T_{1\rho}$  values by the original and modified model as  $N_{sp}$  increases from 1 to 50. The red dashed line highlights the simulated  $T_{1\rho}$ , and the blue squares and green circles represent the  $T_{1\rho}$  values obtained from fitting the original and modified models, respectively. The columns represented 3 groups data with simulated  $T_{1\rho}$  values of 30 (A and D), 60 (B and E), and 90 ms (C and F)

### 3.6 | Data analysis

The Levenberg-Marquardt algorithm was used to fit Eqs. 1 to (3). All analysis algorithms were written in MATLAB (The MathWorks, Natick, MA) and were executed offline on the DICOM images obtained by the acquisition protocols described above. For each fitting of Eqs. 1 and 2, both the  $T_{1\rho}$  value and its fitting error were calculated. ROIs were manually drawn for various tissues including quadriceps tendon, patellar tendon, ACL, PCL, meniscus, patellar cartilage, and muscle in all ex vivo and in vivo knee joints.

## 4 | RESULTS

Numerical simulations for the fitting model study are shown in Figure 2. As shown in Figures 2A–2C, the Bloch equation simulated data with different  $N_{sp}$  per Adiab $T_{1\rho}$  preparation have different signal intensities. The data fitting with the original model of Eq. 1 and modified model of Eq. 2 were excellent in all simulations. However, as shown in Figures 2D–2F, the calculated  $T_{1\rho}$  values using the original model were dependent on the  $N_{sp}$ . As expected, the calculated  $T_{1\rho}$  values increased with higher  $N_{sp}$  using the original model. In contrast,  $T_{1\rho}$  values calculated by the modified model were

very close to the true simulated value independent of the  $N_{sp}$ , suggesting improved accuracy of the modified model.

Figure 3 shows the agarose phantom results for the fitting model study. The data acquisition time was significantly reduced when a higher  $N_{sp}$  was used. As shown in Figure 3B, the phantom data acquired with different  $N_{sp}$  per Adiab $T_{1\rho}$  preparation have different signal intensities, similar to the simulation study. The obtained  $T_{1\rho}$  values calculated by the original model significantly increased with a higher  $N_{sp}$ . In contrast, the  $T_{1\rho}$  values calculated by the modified model only increased very slightly with a higher  $N_{sp}$ , which further demonstrated the accuracy of the modified model. The average coefficient of variation for the Adiab $T_{1\rho}$  UTE-Cones scan of the agarose phantom on 4 repeated acquisitions was  $< 3\%$ , demonstrating good reproducibility of the technique.

Supporting Information Figure S1 shows the magic angle effect in Adiab $T_{1\rho}$  UTE-Cones imaging of a sliced patellar sample. Significant signal intensity changes can be found in the localizer images with different angular orientations between the normal direction of cartilage surface and  $\vec{B}_0$ . Excellent fitted curves using the modified signal model were obtained for each angle. Figure 4 shows how the calculated  $T_{1\rho}$  values vary with orientation angle, with CPMG-derived  $T_2$  values included for comparison. Whereas the  $T_2$  value

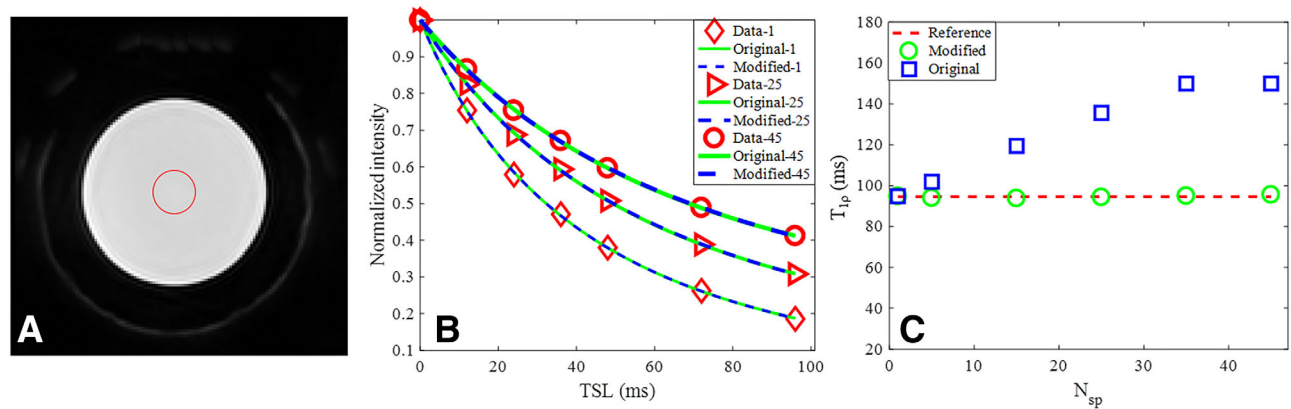


**FIGURE 3** 3D Adiab $T_{1\rho}$  UTE-Cones of a 2% agarose phantom with 0.1 mM  $MnCl_2$ . (A) The region of interest for analysis is shown as the red circle on a selected Adiab $T_{1\rho}$  image ( $N_{sp} = 25$ ,  $N_{AFP} = 4$ ). (B) Original and modified signal model fitting. The red diamond, triangle, and circle markers represent the phantom data with 1, 25, and 45 spokes per Adiab $T_{1\rho}$  preparation, respectively. (C) Calculated  $T_{1\rho}$  values by the original and modified models as  $N_{sp}$  increases from 1 to 50. The red dashed line is the reference  $T_{1\rho}$  obtained with  $N_{sp} = 1$ , and the blue squares and green circles in represent the  $T_{1\rho}$  values obtained from the fitting by original and modified model, respectively

increased by  $\sim 200\%$  as the angle increased from  $0^\circ$  to  $55^\circ$ , the calculated  $T_{1\rho}$  values only increased by  $\sim 50\%$ .

Figure 5 shows the results of the ex vivo whole knee study of a 63-year-old female donor. The 3D Adiab $T_{1\rho}$  UTE-Cones sequence provides high signal and contrast imaging of long  $T_2$  tissues such as the articular cartilage and muscle, together with short  $T_2$  tissues of meniscus, quadriceps tendon, patellar tendon, ACL, and PCL (Figures 5A–5C). Excellent  $T_{1\rho}$  fitting of the 3D Adiab $T_{1\rho}$  UTE-Cones images with different TSLs (Figures 5D–5F) demonstrates a  $T_{1\rho}$  of  $24.5 \pm 1.3$  ms for the quadriceps tendon,  $38.8 \pm 3.2$  ms for the PCL,  $33.2 \pm 1.3$  ms for the meniscus, and  $55.6 \pm 5.2$  ms for the patellar cartilage.

Figure 6 shows the results of an in vivo whole knee study of a 23-year-old male volunteer. Similar to the ex vivo sample study, the 3D Adiab $T_{1\rho}$  UTE-Cones sequence also provides high signal and contrast imaging of both short and long  $T_2$  tissues in the whole knee joint (Figures 6A–6C). Excellent Adiab $T_{1\rho}$  fitting of the 3D Adiab $T_{1\rho}$  UTE-Cones

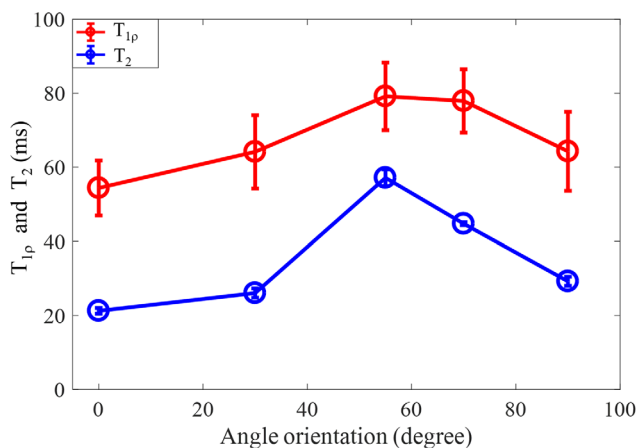
images with different TSLs (Figures 6D–6F) demonstrates a  $T_{1\rho}$  of  $13.7 \pm 1.0$  ms for the quadriceps tendon,  $22.5 \pm 1.2$  ms for the PCL,  $21.5 \pm 1.1$  ms for the meniscus, and  $43.5 \pm 5.9$  ms for the patellar cartilage.

Table 1 summarizes the  $T_{1\rho}$  values for quadriceps tendon, patellar tendon, ACL, PCL, meniscus, patellar cartilage, and muscle for the 4 ex vivo knee images and the 6 in vivo knee images. Relatively consistent  $T_{1\rho}$  values were derived for each knee tissue within each experiment, although the ex vivo  $T_{1\rho}$  values are consistently higher than the corresponding in vivo  $T_{1\rho}$  values.

## 5 | DISCUSSION

We have demonstrated in this study that the proposed 3D Adiab $T_{1\rho}$  UTE-Cones sequence can provide reliable volumetric  $T_{1\rho}$  assessment of both short and long  $T_2$  tissues in whole knee imaging on a clinical 3T scanner. Our simulation and phantom studies suggest that the modified signal model is more preferred for the time-efficient multispoke acquisition than the original signal model. Furthermore, the magic angle study using a sliced human patellar cartilage sample demonstrated that the  $T_{1\rho}$  values generated from the 3D Adiab $T_{1\rho}$  UTE-Cones technique were much less sensitive to the magic angle effect than CPMG-derived  $T_2$  values, and compared with CW- $T_{1\rho}$  values from previous studies.<sup>12,13</sup> Our ex vivo and in vivo whole knee studies demonstrate its feasibility in quantifying  $T_{1\rho}$  for quadriceps tendon, patellar tendon, ACL, PCL, meniscus, patellar cartilage, and muscle.

Knee OA is recognized as a whole organ disease. Previous studies have shown that failure of any component, such as meniscal positioning or collateral ligament damage, can lead to cartilage loss.<sup>24,25,37</sup> In general, the deterioration or misalignment of any of the tissues comprising the knee joint



**FIGURE 4** Comparison of magic angle effect for cartilage  $T_{1\rho}$  values from 3D Adiab $T_{1\rho}$  UTE-Cones and  $T_2$  values from a CPMG sequence

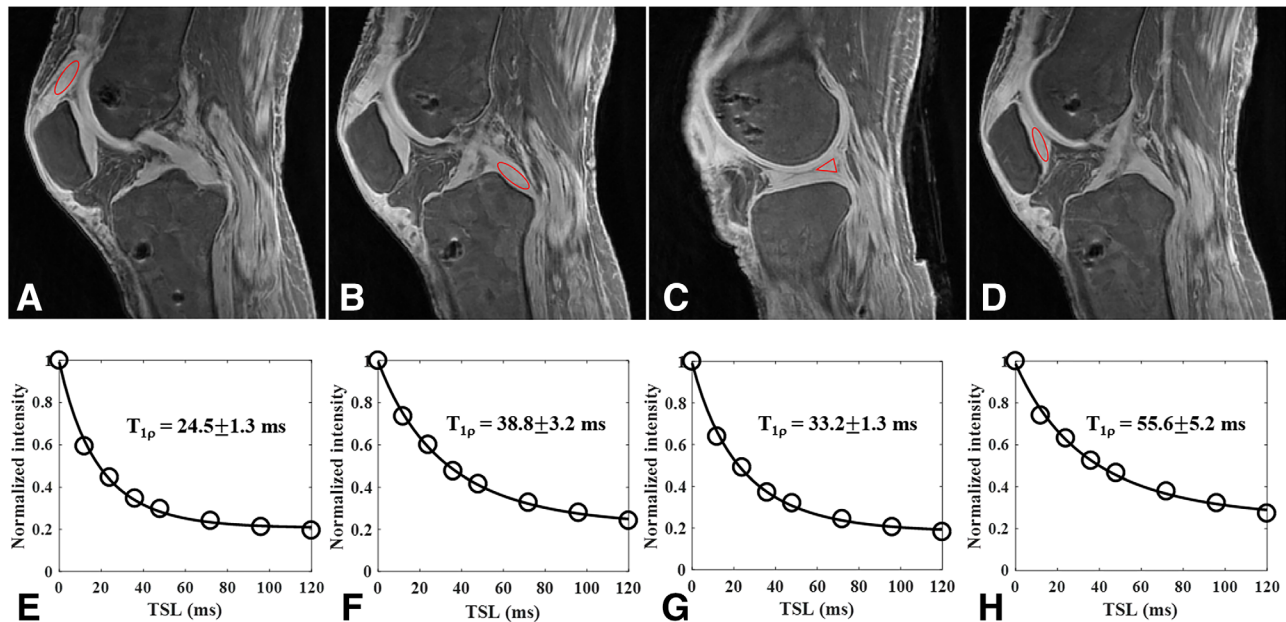


**FIGURE 5** 3D Adiab $T_{1p}$  UTE-Cones imaging of an ex vivo knee sample (63-year-old female donor). Representative Adiab $T_{1p}$  images with regions of interest (red circles) and corresponding fitting curves of quadriceps tendon, PCL, meniscus, and patellar cartilage are shown in the first and second rows, respectively. The  $T_{1p}$  values of quadriceps tendon, PCL, meniscus, and patellar cartilage were  $24.5 \pm 1.3$ ,  $38.8 \pm 3.2$ ,  $33.2 \pm 1.3$ , and  $55.6 \pm 5.2$  ms, respectively

can accelerate the progression of OA.<sup>23–25,37</sup> As such, it is essential to image all major components in the knee joint to allow for comprehensive assessment of OA. In this study, we demonstrate that the 3D Adiab $T_{1p}$  UTE-Cones sequence can image and calculate  $T_{1p}$  values for all the major components in the knee joint including both short and long  $T_2$  tissues.

Recent studies have shown that Adiab $T_{1p}$  is sensitive to both ex vivo enzymatic cartilage degradation and in vivo articular cartilage degradation in OA patients.<sup>18,38,39</sup> More importantly, the Adiab $T_{1p}$  is much less sensitive to the magic angle effect than both conventional CW- $T_{1p}$  and  $T_2$  as demonstrated in previous bovine cartilage studies.<sup>19,20</sup> Our

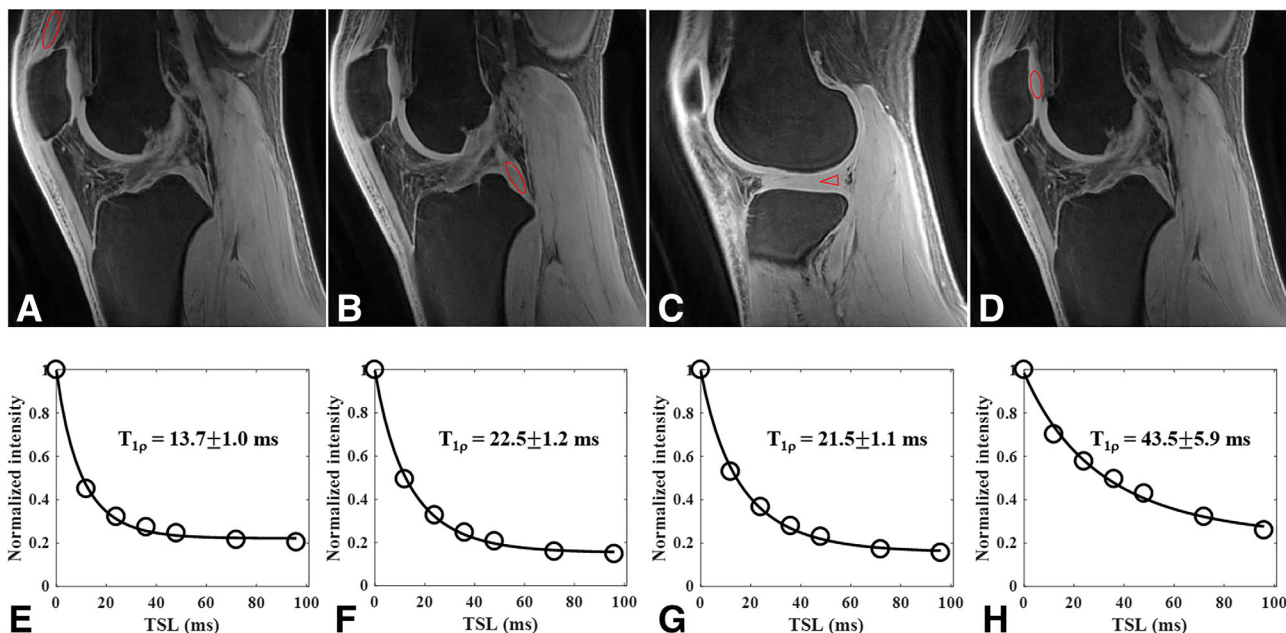


**FIGURE 6** 3D Adiab $T_{1p}$  UTE-Cones imaging of an in vivo healthy knee (23-year-old male volunteer). Representative Adiab $T_{1p}$  images with regions of interest (red circles) and corresponding fitting curves of quadriceps tendon, PCL, meniscus, and patellar cartilage are shown in the first and second rows, respectively. The  $T_{1p}$  values of quadriceps tendon, PCL, meniscus, and patellar cartilage were  $13.7 \pm 1.0$ ,  $22.5 \pm 1.2$ ,  $21.5 \pm 1.1$ , and  $43.5 \pm 5.9$  ms, respectively



**TABLE 1**  $T_{1\rho}$  and its fitting standard errors (ms) of quadriceps tendon, patellar tendon, ACL, PCL, meniscus, patellar cartilage and muscles in 4 ex vivo human knee samples as well as their average and SD values (ms)

Ex vivo knee	1	2	3	4	Average
Quadriceps tendon	24.5 ± 1.3	21.9 ± 1.8	23.8 ± 2.0	19.5 ± 1.5	22.5 ± 2.2
Patellar tendon	22.5 ± 1.5	26.4 ± 3.1	23.2 ± 2.5	17.5 ± 1.7	22.4 ± 3.7
ACL	45.8 ± 2.0	53.2 ± 8.9	49.3 ± 5.3	45.2 ± 5.4	48.4 ± 3.7
PCL	38.8 ± 3.2	38.9 ± 4.5	44.3 ± 3.9	38.5 ± 4.0	40.1 ± 2.8
Meniscus	33.2 ± 1.3	36.8 ± 3.7	33.7 ± 2.9	34.8 ± 3.6	34.6 ± 1.6
Patellar cartilage	55.6 ± 5.2	59.7 ± 9.8	58.7 ± 10.2	44.3 ± 6.4	54.6 ± 7.0
Muscle	60.9 ± 4.1	55.3 ± 8.1	58.6 ± 6.4	51.8 ± 6.3	56.7 ± 4.0

human patellar cartilage study extends these findings to 3D UTE-Cones adapted Adiab $T_{1\rho}$  sequences. The combination of  $T_{1\rho}$  preparation with UTE sequences can also be used to quantify other clinically meaningful short  $T_2$  tissues in the knee joint such as the meniscus.<sup>40–42</sup> The meniscus plays an important role in normal knee function, and there is high interest in evaluating degenerative changes in the meniscus with  $T_{1\rho}$  sequences.<sup>40–42</sup> For example, Rauscher et al.<sup>40</sup> reported a high correlation between meniscal  $T_{1\rho}$  and clinical findings of OA, suggesting the importance of  $T_{1\rho}$  imaging of the meniscus. However, only long  $T_2$  components in the meniscus could be quantified in that study because they used clinical gradient echo sequences with TEs around 4 ms, which are too long to detect the short  $T_2$  components that comprise a significant proportion of the meniscus. Therefore, the 3D Adiab $T_{1\rho}$  UTE-Cones sequence is likely to provide a more accurate assessment of cartilage degeneration in the meniscus compared to the magic angle sensitive CW- $T_{1\rho}$  sequence based on conventional gradient echo sequences.<sup>40–42</sup>

In addition to lower RF power deposition compared with CW- $T_{1\rho}$  prepared sequences, the proposed Adiab $T_{1\rho}$  UTE-Cones sequence is more resistant to both  $B_1$  and  $B_0$  inhomogeneities because of the adiabatic pulse character and relatively broad pulse spectral coverage of 1.643 kHz. Therefore, Adiab $T_{1\rho}$  prepared sequences will also be preferred over CW- $T_{1\rho}$  prepared sequences in high field MRI where these effects are more significant. In addition to the HS1 type of AFP pulse used in this study, other RF types such as HS4 and HS8 can also be designed for Adiab $T_{1\rho}$  preparation.<sup>15,18,20</sup> Different  $T_{1\rho}$  characters can be generated by different types of RF pulses. For example,  $T_{1\rho}$  generated by HS4 type pulse trains is slightly more sensitive to cartilage degeneration but also more sensitive to the magic angle effect compared with the  $T_{1\rho}$  generated by HS1 type pulse trains.<sup>20</sup>

Significant scan time reduction for the 3D Adiab $T_{1\rho}$  UTE-Cones sequence was achieved using multispoke data

acquisition in this study. Both simulation and phantom studies demonstrated that the modified signal model of Eq. 2 was appropriate for  $T_{1\rho}$  fitting by incorporating saturation effects during the multispoke acquisition. A low flip angle was used for signal excitation to avoid image artifacts induced by the signal intensity variations among the acquisition spokes. As can be seen from both phantom (Figure 3) and knee data (Figures 5 and 6), an interesting phenomenon was observed: the signal intensity of the data acquired with an Adiab $T_{1\rho}$  preparation of a non MLEV4 phase scheme (e.g.,  $N_{AFP} = 2$  or 6) was still located properly along the fitting curve. This suggests that heteronuclear decoupling with a MLEV4 phase scheme is not necessary for Adiab $T_{1\rho}$  contrast generation.

There is an important difference between our sequence and the sequence recently reported by Zhang et al.<sup>21</sup> for 3D adiabatic  $T_{1\rho}$  mapping. In our sequence, to increase the SNR, there is a gap between the end of the acquisition spoke series and the next Adiab $T_{1\rho}$  preparation. However, no such gap exists in the Zhang et al.<sup>21</sup> sequence, because they used a high field animal scanner that has much better SNR performance. In addition, whereas Zhang et al.<sup>21</sup> used a semi-analytical approach, we used a simplified model because the accurate signal equation can be even more complicated than the Zhang et al.<sup>21</sup> signal equation. However, as demonstrated by both simulation and phantom studies, we can still get good fitting results with our simplified signal model. As shown in the fitting curves in both Figures 5 and 6, the data of all the tissues in the knee fit the mono-exponential model well. Different proton pools in a tissue are likely to have different  $T_{1\rho}$  values, and in particular, the extremely short  $T_2$  proton components may have shorter  $T_{1\rho}$  values. However, AFP pulses cannot be made short enough to get the Adiab $T_{1\rho}$  signal decay curve for the extremely short  $T_2$  components because of the limitation of both RF peak power and specific absorption rate (SAR) levels in clinical scanners. A relatively high peak  $B_1$  value was used for the AFP pulses to shorten the RF duration so that more signals from the short  $T_2$  tissues (such as meniscus) can be acquired. SAR will be

**TABLE 2**  $T_{1\rho}$  and its fitting standard errors (ms) of quadriceps tendon, patellar tendon, ACL, PCL, meniscus, patellar cartilage and muscles in 6 in vivo human knee samples as well as their average and SD values (ms)

In vivo knee	1	2	3	4	5	6	Average
Quadriceps tendon	13.6 ± 0.6	13.4 ± 1.1	13.6 ± 1.0	14.9 ± 1.3	13.7 ± 1.0	12.9 ± 1.2	13.9 ± 0.7
Patellar tendon	9.3 ± 0.5	9.3 ± 0.4	9.4 ± 0.3	9.6 ± 0.7	9.4 ± 0.5	11.3 ± 0.6	9.7 ± 0.8
ACL	35.0 ± 4.5	37.3 ± 3.8	33.4 ± 3.5	37.5 ± 5.6	36.1 ± 3.9	30.0 ± 3.0	34.9 ± 2.8
PCL	21.5 ± 1.9	22.9 ± 1.7	21.2 ± 2.0	22.6 ± 1.7	22.5 ± 1.2	19.0 ± 1.5	21.6 ± 1.4
Meniscus	23.0 ± 1.6	21.3 ± 1.4	26.2 ± 1.9	21.4 ± 1.7	21.5 ± 1.1	21.7 ± 1.6	22.5 ± 1.9
Patellar cartilage	42.3 ± 6.5	47.7 ± 6.9	47.3 ± 7.5	42.5 ± 6.6	43.5 ± 5.9	44.1 ± 6.2	44.5 ± 2.4
Muscle	43.7 ± 4.8	42.0 ± 4.7	41.8 ± 4.2	43.7 ± 4.8	44.5 ± 3.2	43.5 ± 4.4	43.2 ± 1.1

increased because of the relatively high RF power. However, the SAR level of the proposed protocol is still in the safe range for extremity imaging where the use of multispokes and a transmit/receive 8-channel knee coil help reduce SAR.

The FatSat pulse will saturate part of tissue magnetizations especially for short  $T_2$  tissues, leading to reduced SNR. However, in UTE imaging with radial or spiral sampling, chemical shift artifacts manifest as ringing artifacts, which will affect the quantitative measurement. Therefore, it is preferred to lose some image SNRs using a FatSat pulse rather than get inaccurate  $T_{1\rho}$  values. Fat saturation time was counted in the non-spin-lock time (i.e.,  $TR - TSL$ ) in the equation. Moreover, with Bloch simulation, we found that placing the fat saturation time between the Adiab $T_{1\rho}$  preparation, and the acquisition spokes has similar fitting results compared to when we placed the fat saturation time right before the Adiab $T_{1\rho}$  preparation. This is because the fat saturation time is much shorter than  $TR$  in this study. Additionally, coil ring-down time should be considered in the definition of the shortest echo time, which is very important for accurate  $T_2^*$  quantification of short  $T_2$  tissues. However, the majority of UTE articles published so far have used the definition of  $TE$  as the time between the end of the short rectangular pulse and the start of k-space center. We have chosen to follow that convention in this article. Furthermore, because we used the same echo time for all the Adiab $T_{1\rho}$  preparations, the image contrasts are mainly generated by these Adiab $T_{1\rho}$  preparations. Therefore, even when contaminated with coil ring-down effects, we can still get accurate quantitative  $T_{1\rho}$  values.

In general, as can be seen from Tables 1 and 2, the  $T_{1\rho}$  values of the tissues measured in the in vivo knee study were consistently lower than the values in the ex vivo knee study. These differences likely reflect the differences in temperature during imaging. The faster  $T_{1\rho}$  decay in vivo may be caused by the stronger spin or molecular fluctuations at the higher temperature of volunteer knee joints than cadaveric knee joints. Because this work focused on technical development,

we only reported the feasibility of  $T_{1\rho}$  quantification for most of the tissues about the knee joint, including tendons, ligaments, meniscus, cartilage, and muscles. We are planning to perform a more systematic magic angle imaging study for cartilage, including the different layers (superficial, transitional, radial, and calcified layers), with several quantitative MRI techniques including  $T_{1\rho}$ ,  $T_2$ , and MT modeling.<sup>43</sup>

This study has several limitations. First, we have only demonstrated the technical feasibility of the 3D Adiab $T_{1\rho}$  UTE-Cones sequence in providing volumetric quantitative  $T_{1\rho}$  imaging of both short and long  $T_2$  tissues both ex vivo and in vivo. No patients were studied in this work. Second, the sensitivity of 3D Adiab $T_{1\rho}$  UTE-Cones measurements to knee joint degeneration has not been investigated. It will be necessary to conduct a systematic study of knee joints with different degrees of degeneration followed by histological evaluation. Third, the 3D Adiab $T_{1\rho}$  UTE-Cones sequence used for in vivo imaging was ~18 min long, which is still relatively long for a patient study. The scan time can be further reduced with a smaller number of TSLs, such as 4. Moreover, fast 3D acquisition with acceleration techniques such as parallel imaging or compressed sensing can be used to further accelerate the data acquisition.<sup>44</sup> Fourth, only patellar cartilage was used for this magic angle study. Other tissues, such as Achilles tendon, menisci, and ligaments, would also be very interesting for future magic angle studies.<sup>43,45</sup>

## 6 | CONCLUSION

The 3D Adiab $T_{1\rho}$  UTE-Cones technique provides robust volumetric quantitative  $T_{1\rho}$  measurement of both short and long  $T_2$  tissues including quadriceps tendon, patellar tendon, ACL, PCL, meniscus, patellar cartilage, and muscle in the knee joint.

## ACKNOWLEDGMENTS

The authors acknowledge grant support from GE Healthcare, NIH (T32EB005970, 1R01 AR062581, and 1R01

AR068987 and) and the VA Clinical Science R&D Service (1I01CX001388).

## REFERENCES

- [1] Grushko G, Schneiderman R, Maroudas A. Some biochemical and biophysical parameters for the study of the pathogenesis of osteoarthritis: a comparison between the processes of aging and degeneration in human hip cartilage. *Connect Tissue Res.* 1989; 19:149-176.
- [2] Duvvuri U, Reddy R, Patel SD, Kaufman JH, Kneeland JB, Leigh JS. T1rho-relaxation in articular cartilage: effects of enzymatic degradation. *Magn Reson Med.* 1997;38:863-867.
- [3] Regatte RR, Akella SVS, Lonner JH, Kneeland JB, Reddy R. T1ρ relaxation mapping in human osteoarthritis (OA) cartilage: comparison of T1ρ with T2. *J Magn Reson Imaging.* 2006;23: 547-553.
- [4] Li X, Han ET, Ma B, Link TM, Newitt DC, Majumdar S. In vivo 3T spiral imaging based multi-slice T1ρ mapping of knee cartilage in osteoarthritis. *Magn Reson Med.* 2005;54:929-936.
- [5] Knispel RR, Thompson RT, Pintar MM. Dispersion of proton spin-lattice relaxation in tissues. *J Magn Reson.* 1974;14:44-51.
- [6] Regatte RR, Akella SVS, Borthakur A, Kneeland JB, Reddy R. Proteoglycan depletion-induced changes in transverse relaxation maps of cartilage. *Acad Radiol.* 2002;9:1388-1394.
- [7] Duvvuri U, Charagundla SR, Kudchodkar SB, et al. Human knee: in vivo T1ρ-weighted MR imaging at 1.5 T - preliminary experience. *Radiology.* 2001;220:822-826.
- [8] Mlynarik V, Szomolanyi P, Toffanin R, Vittur F, Trattnig S. Transverse relaxation mechanisms in articular cartilage. *J Magn Reson.* 2004;169:300-307.
- [9] Rautiainen J, Nissi MJ, Salo EN, et al. Multiparametric MRI assessment of human articular cartilage degeneration: correlation with quantitative histology and mechanical properties. *Magn Reson Med.* 2015;74:249-259.
- [10] Akella SV, Regatte RR, Wheaton AJ, Borthakur A, Reddy R. Reduction of residual dipolar interaction in cartilage by spin-lock technique. *Magn Reson Med.* 2004;52:1103-1109.
- [11] Wang N, Xia Y. Dependencies of multi-component T2 and T1ρ relaxation on the anisotropy of collagen fibrils in bovine nasal cartilage. *J Magn Reson.* 2011;212:124-132.
- [12] Shao H, Pauli C, Li S, et al. Magic angle effect plays a major role in both T1rho and T2 relaxation in articular cartilage. *Osteoarthritis Cartilage.* 2017;25:2022-2030.
- [13] Du J, Statum S, Znamirovski R, Bydder GM, Chung CB. Ultrashort TE T1ρ magic angle imaging. *Magn Reson Med.* 2013;69: 682-687.
- [14] Erickson SJ, Prost RW, Timins ME. The "magic angle" effect: background physics and clinical relevance. *Radiology.* 1993;188: 23-25.
- [15] Garwood M, DelaBarre L. The return of the frequency sweep: designing adiabatic pulses for contemporary NMR. *J Magn Reson.* 2001;153:155-177.
- [16] Michaeli S, Grohn H, Grohn O, et al. Exchange-influenced T2rho contrast in human brain images measured with adiabatic radio frequency pulses. *Magn Reson Med.* 2005;53:823-829.
- [17] Michaeli S, Sorce DJ, Springer CS Jr, Ugurbil K, Garwood M. T1rho MRI contrast in the human brain: modulation of the longitudinal rotating frame relaxation shutter-speed during an adiabatic RF pulse. *J Magn Reson.* 2006;181:135-147.
- [18] Casula V, Autio J, Nissi MJ, et al. Validation and optimization of adiabatic T1ρ and T2ρ for quantitative imaging of articular cartilage at 3T. *Magn Reson Med.* 2017;77:1265-1275.
- [19] Nissi MJ, Mangia S, Michaeli S, Nieminen MT. Orientation anisotropy of rotating frame and T2 relaxation parameters in articular cartilage. In: Proceedings of the 21st Annual Meeting of ISMRM, Salt Lake City, UT, 2013. Abstract 3552.
- [20] Hänninen N, Rautiainen J, Rieppo L, Saarakkala S, Nissi MJ. Orientation anisotropy of quantitative MRI relaxation parameters in ordered tissue. *Sci Rep.* 2017;7:9606.
- [21] Zhang J, Nissi MJ, Idiyatullin D, Michaeli S, Garwood M, Ellermann J. Capturing fast relaxing spins with SWIFT adiabatic rotating frame spin-lattice relaxation (T1ρ) mapping. *NMR Biomed.* 2016;1;29:420-430.
- [22] Chen W. Errors in quantitative T1rho imaging and the correction methods. *Quant Imaging Med Surg.* 2015;5:583-591.
- [23] Brandt KD, Radin EL, Dieppe PA, Putte L. Yet more evidence that osteoarthritis is not a cartilage disease (Editorial). *Ann Rheum Dis.* 2006;65:1261-1264.
- [24] Hunter DJ, Zhang YQ, Niu JB, et al. The association of meniscal pathologic changes with cartilage loss in symptomatic knee osteoarthritis. *Arthritis Rheum.* 2006;54:795-801.
- [25] Tan AL, Toumi H, Benjamin M, et al. Combined high-resolution magnetic resonance imaging and histological examination to explore the role of ligaments and tendons in the phenotypic expression of early hand osteoarthritis. *Ann Rheum Dis.* 2006;65:1267-1272.
- [26] Chang EY, Du J, Bae WC, Chung CB. Qualitative and quantitative ultrashort echo time imaging of musculoskeletal tissues. *Semin Musculoskelet Radiol.* 2015;19:375-386.
- [27] Du J, Carl M, Diaz E, et al. Ultrashort TE T1rho (UTE T1rho) imaging of the Achilles tendon and meniscus. *Magn Reson Med.* 2010;64:834-842.
- [28] Du J, Carl M, Bae WC, et al. Dual inversion recovery ultrashort echo time (DIR-UTE) imaging and quantification of the zone of calcified cartilage (ZCC). *Osteoarthritis Cartilage.* 2013;21:77-85.
- [29] Ma YJ, Carl M, Shao H, Tadros AS, Chang EY, Du J. Three-dimensional ultrashort echo time cones T1ρ (3D UTE-cones-T1ρ) imaging. *NMR Biomed.* 2017;30.
- [30] Gurney PT, Hargreaves BA, Nishimura DG. Design and analysis of a practical 3D cones trajectory. *Magn Reson Med.* 2006;55: 575-582.
- [31] Carl M, Bydder GM, Du J. UTE imaging with simultaneous water and fat signal suppression using a time-efficient multi-spoke inversion recovery pulse sequence. *Magn Reson Med.* 2016;76:577-582.
- [32] Levitt MH, Freeman R, Frenkiel T. Supercycles for broad-band heteronuclear decoupling. *J Magn Reson.* 1982;50:157-160.
- [33] Ma YJ, Chang EY, Carl M, Du J. Quantitative magnetization transfer ultrashort echo time imaging using a time-efficient 3D multispoke Cones sequence. *Magn Reson Med.* 2018;79:692-700.

- [34] Fram EK, Herfkens RJ, Johnson GA, et al. Rapid calculation of T1 using variable flip angle gradient refocused imaging. *Magn Reson Imaging*. 1987;5:201-208.
- [35] Ma YJ, Lv X, Carl M, et al. Accurate T1 mapping of short T2 tissues using a three-dimensional ultrashort echo time cones actual flip angle imaging variable repetition time (3D UTE-Cones AFI-VTR) method. *Magn Reson Med*. 2018;80:598-608.
- [36] Ma YJ, Zhu Y, Lu X, Carl M, Chang EY, Du J. Short T2 imaging using a 3D double adiabatic inversion recovery prepared ultrashort echo time cones (3D DIR-UTE-Cones) sequence. *Magn Reson Med*. 2018;79:2555-2563.
- [37] Hunter DJ, Zhang Y, Niu J, et al. Structural factors associated with malalignment in knee osteoarthritis: the Boston osteoarthritis knee study. *J Rheumatol*. 2005;32:2192-2199.
- [38] Nissi MJ, Salo EN, Tiitu V, et al. Multi-parametric MRI characterization of enzymatically degraded articular cartilage. *J Orthopaedic Research*. 2016;34:1111-1120.
- [39] Casula V, Nissi MJ, Podlipská J, et al. Elevated adiabatic T1 $\rho$  and T2 $\rho$  in articular cartilage are associated with cartilage and bone lesions in early osteoarthritis: a preliminary study. *J Magn Reson Imaging*. 2017;46:678-689.
- [40] Rauscher I, Stahl R, Cheng J, et al. Meniscal measurements of T1rho and T2 at MR imaging in healthy subjects and patients with osteoarthritis. *Radiology*. 2008;249:591-600.
- [41] Bolbos RI, Link TM, Ma CB, Majumdar S, Li X. T1rho relaxation time of the meniscus and its relationship with T1rho of adjacent cartilage in knees with acute ACL injuries at 3 T. *Osteoarthritis Cartilage*. 2009;17:12-18.
- [42] Wang L, Chang G, Bencardino J, et al. T1rho MRI of menisci in patients with osteoarthritis at 3 Tesla: a preliminary study. *J Magn Reson Imaging*. 2014;40:588-595.
- [43] Ma YJ, Shao H, Du J, Chang EY. Ultrashort echo time magnetization transfer (UTE-MT) imaging and modeling: magic angle independent biomarkers of tissue properties. *NMR Biomed*. 2016;29:1546-1552.
- [44] Pandit P, Rivoire J, King K, Li X. Accelerated T1 $\rho$  acquisition for knee cartilage quantification using compressed sensing and data-driven parallel imaging: a feasibility study. *Magn Reson Med*. 2016;75:1256-1261.
- [45] Henkelman RM, Stanisz GJ, Kim JK, Bronskill MJ. Anisotropy of NMR properties of tissues. *Magn Reson Med*. 1994;32:592-601.

## SUPPORTING INFORMATION

Additional Supporting Information may be found in the online version of this article.

**FIGURE S1** Patellar cartilage sample images used to study the magic angle effect on 3D AdiabT $_{1\rho}$  UTE-Cones. Localizers, AdiabT $_{1\rho}$  images, and corresponding fitting curves of 5 angular orientations (0°, 30°, 55°, 70°, and 90° between the normal direction of cartilage surface and the main field  $\vec{B}_0$ ) are shown. The localizer was imaged by a conventional GRE sequence with TE/TR = 3.2/8.6 ms. The selected AdiabT $_{1\rho}$  images were acquired with N $_{AFP}$  = 0, 4, 8, and 16. The obtained T $_{1\rho}$  values are shown together with the fitting curves.

**How to cite this article:** Ma Y-J, Carl M, Searleman A, Lu X, Chang EY, Du J. 3D adiabatic T $_{1\rho}$  prepared ultrashort echo time cones sequence for whole knee imaging. *Magn Reson Med*. 2018;80:1429–1439. <https://doi.org/10.1002/mrm.27131>